Iranian Journal of Geophysics, Vol 19 No 6, 2026, Page 125 – 138 (Research Article)
DOI: 10.30499/ijg.2025.480141.1638

Determining apparent source time function (ASTF) of seismic events through empirical green function analysis (a case study of Khoy 2023 earthquake)

Khalil Bakhtiari Asl[1*], Vladimir Plicka[2] and Khosro Moghtased- Azar[3]

[1] *M.Sc., Department of Geomatics Engineering, Faculty of Civil Engineering, University of Tabriz, Tabriz, Iran*
[2] *Ph.D., Department of Geophysics, Faculty of Mathematics and Physics, Charles University, Prague, Czech Republic*
[3] *Associate Professor, Department of Geomatics Engineering, Faculty of Civil Engineering, University of Tabriz, Tabriz, Iran*

(Received: 26 Septeber 2024, Accepted: 07 February 2025)

Abstract

The study examines the Apparent Source Time Function (ASTF) for four seismic stations (MRD, SDS1, URUN, and MAHB) in relation to the Khoy earthquake. By employing the method developed by (Plicka, et al. 2022), we meticulously calculate the ASTFs to investigate the temporal distribution of seismic energy release during the earthquake. Our analysis reveals significant variations in ASTF duration across the different stations. Specifically, the MRD station exhibits a notably short ASTF duration of 5 seconds, whereas the URUN station shows a considerably longer ASTF duration of 18 seconds. The SDS1 and MAHB stations fall in between, with ASTF durations of 15 seconds and 12 seconds, respectively. These observed variations in ASTF durations likely indicate differences in fault properties and rupture dynamics at each station. The shorter ASTF at MRD may suggest a more abrupt energy release, while the longer ASTF at SDS1 could imply a more prolonged rupture process. The intermediate durations at URUN and MAHB further highlight the complexity and variability of seismic energy release mechanisms. Our findings contribute valuable insights into seismic hazard assessment and fault characterization in the Khoy region. By applying the ASTF calculation method to this specific case study, we demonstrate its utility in enhancing our understanding of earthquake dynamics. This innovative application underscores the importance of ASTF analysis in seismic studies and its potential to inform more accurate seismic hazard models. Furthermore, our research opens up new avenues for future investigations. We suggest that subsequent studies should focus on a broader range of seismic events and stations to validate and refine the ASTF method. Additionally, exploring the relationship between ASTF characteristics and other seismic parameters, such as fault slip and rupture velocity, could provide deeper insights into the underlying mechanisms of earthquake generation. In conclusion, this study not only advances our knowledge of the Khoy earthquake but also highlights the broader applicability of ASTF analysis in seismology. Our work underscores the need for continued research in this area to improve seismic hazard assessments and enhance our understanding of earthquake processes. By integrating ASTF analysis with other geophysical methods, we can develop a more comprehensive picture of seismic activity, ultimately contributing to better preparedness and mitigation strategies in earthquake-prone regions. This holistic approach will be crucial for advancing the field of seismology and ensuring the safety and resilience of communities affected by seismic events. The insights gained from this study can also be applied to other regions with similar seismic profiles, thereby broadening the impact and relevance of our findings.

Keywords: Apparent source time function, earthquake source parameter estimation, EGF

[*]Corresponding author: khalilbakhtiariasl1998@gmail.com

1 Introduction

Seismology, a branch of geophysics, involves the systematic study of earthquakes and the propagation of elastic waves through the Earth. This field is essential for understanding the behavior and characteristics of seismic events, which in turn supports vital risk assessment efforts. One of the fundamental goals in seismology is to accurately determine the origin, magnitude, and focal mechanisms of earthquakes. (Stein and Wysession 2009).

The Apparent Source Time Function (ASTF) is a seismological concept used to describe the shape of a waveform as it appears at a seismic station (López-Comino, et al. 2012). According to Newton's Third Law and considering the diverse forms and materials within various geological layers, the response of these layers to earthquake waves (acting as the external force) will naturally differ. The interactions between the earthquake waves and the geological layers generate anomalies that impact the original waveforms, such as attenuation and scattering. These effects can alter the shape of the original signal, thereby hindering the acquisition of accurate and precise information about the Earth's internal layers.

The ASTF method aims to model and describe distortions, providing insights into the characteristics of the seismic source and Earth's structure. The Empirical Green's Function (EGF) method has been extensively used in seismology to calculate the Apparent Source Time Function (ASTF) (Hough 1997). This approach involves determining source parameters through standard EGF deconvolution and then performing an inversion to obtain a common attenuation parameter for a series of collocated events(Hough, et al. 1999).

(Mueller 1985) improved the analysis of earthquake source-time functions by eliminating the complexities introduced by the path, recording site, and instrumentation in seismograms. By assuming that a small earthquake has a simple source, its seismogram can be used as an empirical Green's function. This seismogram is then deconvolved from the seismogram of a larger or more complex earthquake using spectral division.

In a study by (Hutchings, et al. 2012) empirical Green's functions were applied to investigate earthquake sources, wave propagation, and strong ground motion. Their research offered valuable insights into the practical applications of EGFs, enhancing our understanding and ability to predict earthquake behaviors.

(Hutchings 1991) utilized empirical Green's functions to predict strong ground motion for the 1989 Loma Prieta earthquake. This study highlighted the practical application of EGFs in forecasting ground motions during major seismic events, demonstrating their effectiveness in real-world scenarios.

(Courboulex, et al. 1996) conducted a source investigation of a small seismic event using empirical Green's functions and simulated annealing. Their research offered a fresh perspective on the application of EGFs for exploring the source characteristics of minor seismic events.

In the context of the 2020 Samos Mw7 earthquake,(Plicka, et al. 2022) developed a new variant of the empirical Green’s function method. Their research confirmed the prevalence of large slip amplitudes (~2.4 m) along the entire ruptured area, as well as the up-dip and westward rupture propagation.

(Irikura 1984) predicted strong ground motions using observed seismograms from small events. His work demonstrated the potential of using empirical Green's functions (EGFs) in predicting strong ground motions, further underscoring the significance of EGFs in seismological studies.

In conclusion, the Empirical Green's Function (EGF) method has proven to be a valuable tool in calculating the Apparent Source Time Function (ASTF). The development of new methods and techniques, alongside the practical applications of EGFs in predicting ground motions and investigating earthquake sources, has significantly advanced our understanding of seismic behaviors. Future research in this area is likely to continue refining these methods and potentially develop new ones, further enhancing our ability to analyze and predict seismic events.

Different approaches exist to obtain earthquake source parameters. The Green's function serves as a mathematical representation of the elastic medium's response to a point source. It elucidates the transmission of seismic waves from the source to any designated point within the Earth's structure. By comprehending and utilizing the Green's function, seismologists can glean valuable insights into subsurface structures, properties, and the dynamic processes associated with seismic tremors occurring during earthquakes.

To better understand regional tectonic phenomena and the underlying principles of physics, we utilized the empirical Green's function (EGF) technique to determine earthquake source characteristics.

The Empirical Green's Function (EGF) method is used to estimate ground motions resulting from significant earthquakes by utilizing records of smaller seismic events. This approach is based on the premise that minor seismic occurrences contain valuable information about the propagation path of seismic waves and localized effects. Applications of this methodology include determining earthquake source parameters, simulating strong ground motion, predicting ground motion, and facilitating earthquake risk analysis.

In this study, we employed a novel approach to compute "source time functions." The waveforms generated using this method in two primary modes—the main earthquake and the aftershock—were compared to evaluate its efficacy.

2 Data and Case Study

In this study, data from the Institute of Geophysics, University of Tehran, was employed for the Khoy earthquake.

On September 21st, 2022, consecutive earthquakes started in Khoy city, located in West Azerbaijan province, so that on this date, an earthquake with a magnitude of 5 occurred at a longitude of 44.9 east and a latitude of 38.4 north at a depth of 14 kilometers at 22:27' local time. After that, there were four big earthquakes and a large number of aftershocks, according to the report of the National Seismological Center of the Iran Geophysics Institute, 502 earthquakes were recorded in this city until January 30th, 2023. Major earthquakes occurred with a magnitude greater than 5 in this region are listed in Table 1, where the geographical location, time of occurrence, magnitude and depth of the earthquakes are shown. According to USGS, the causative fault for this specific earthquake is believed to

be the North Tabriz Fault, which is a major right-lateral strike-slip fault in the region (Salmanian, et al. 2024).

In this study, the earthquake with the magnitude of 5 mentioned in the table, was used as the mainshock and the earthquake happened in the same day at 20:09 UTC with the latitude of 38.5 and the longitude of 44.8 was used as the aftershock. The locations of these shocks and the Seismic stations used in this study are shown in Figure 1 and the Information and Coordinates of Stations Used for Inversion are shown in table 2.

Table 1. Information of four earthquakes with the magnitude greater than 5 happened in Khoy, West Azerbaijan, Iran.

Date	Sep, 21st , 2022	Oct, 5th, 2020	Jan, 18th, 2023	Jan, 28th, 2023
Time	18:57’	00:21’	10:08’	18:14’
Latitude	38.47	38.49	38.57	38.59
Longitude	45.04	45.03	44.8	44.8
Magnitude	5	5.4	5.4	5.9
Depth (km)	14	11	12	7

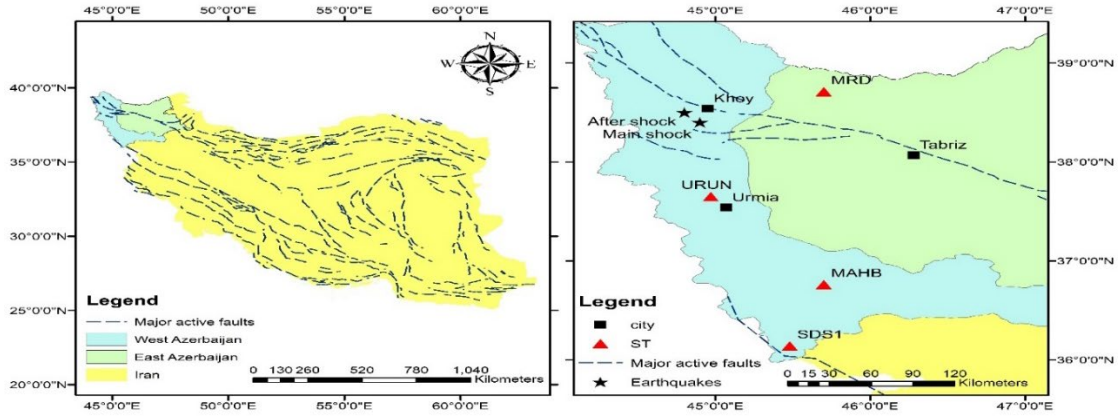

Figure 1. Location of Mainshock and Aftershock around Khoy beside the seismic stations used in this study, Northwest of Iran. The fault trace in the figure are from GEM website.

Table 2. Information and Coordinates of Stations Used for Inversion.

Number	**Station Name**	**Latitude**	**Longitude**	**Distance (km)**	**Instrument Type**
1	MRD	38.71	45.7	76	Broadband
2	MAHB	36.76	45.7	197	Broadband
3	SDS1	36.14	45.48	258	Broadband
4	URUN	37.65	44.97	86	Broadband

3 Methodology

We chose to apply the EGF method as proposed by (Plicka, et al. 2022). The waveforms S_A (t) and S_M (t) corresponding to the weak event (EGF) and the mainshock, respectively, are delineated by Equations (1) and (2):

$$S_A(t) = m(t) * g(t) \quad (1)$$

$$S_M(t) = M(t) * g(t) \quad (2)$$

The functions m (t) and M (t) represent moment rate functions. We posit a frequency range (specified subsequently) within which m (t) can be modeled as an isosceles triangle,

centered at t=0, with a duration shorter than that of $M(t)$.

The function $M(t)$ can be represented as a collection of functions $m(t)$ that are uniformly shifted in time, as detailed in Equation (3), where wi represent undetermined weights. The temporal displacements, denoted by $\tau_i = (i-1)\,\Delta\tau$, and their quantity N are predetermined.

$$M(t) = \sum_{i=1}^{N} m(t - \tau_i) w_i \quad (3)$$

The primary seismic event, denoted as (t), may be expressed as a weighted combination of time-shifted Earthquake Ground Motion (EGM) records:

$$S_M(t) = [\sum_{i=1}^{N} m(t-\tau_i) w_i] * g(t) = \sum_{i=1}^{N} S_A(t-\tau_i) w_i \quad (4)$$

The comparison between the scalar moments of the mainshock and the EGF event (known as the relative moment ratio) helps set limits on the weights.

$$M_0 = \sum_{i=1}^{N} m_0 w_i \,, \frac{M_0}{m_0} = \sum_{i=1}^{N} w_i \quad (5)$$

Expanding these considerations to a three-component station (with a total number of time samples M), Equation (3) with the main earthquake data S and Equation (4) lead to a system of linear algebraic equations for the weights as follows:

$$\begin{pmatrix} S(t_1-\tau_1) & S(t_1-\tau_2) & \cdots & S(t_1-\tau_N) \\ S(t_2-\tau_1) & S(t_1-\tau_2) & \cdots & SS(t_1-\tau_N) \\ . & . & \cdots & . \\ S(t_M-\tau_1) & S(t_1-\tau_2) & \cdots & S(t_1-\tau_N) \\ 1 & 1 & \cdots & 1 \end{pmatrix} \begin{pmatrix} w_1 \\ w_2 \\ . \\ w_N \end{pmatrix} = \begin{pmatrix} S_1 \\ S_2 \\ . \\ S_M \\ \frac{M_0}{m_0} \end{pmatrix} \quad (6)$$

As depicted in Figure 2, the schematic of the study illustrates the process wherein we used broadband seismometers data from IRSC for both the mainshock and aftershocks in three components: NS (North-South), EW (East-West), and Z (vertical). Subsequently, we applied the EGF method to the collected data. Next, employing the NNLS (Non-Negative Least Squares) method, we solved the linear equation system to determine the weights, and ultimately calculated the duration of the ASTF (Apparent Time Series Function). This enabled us to estimate the synthetic waveform.

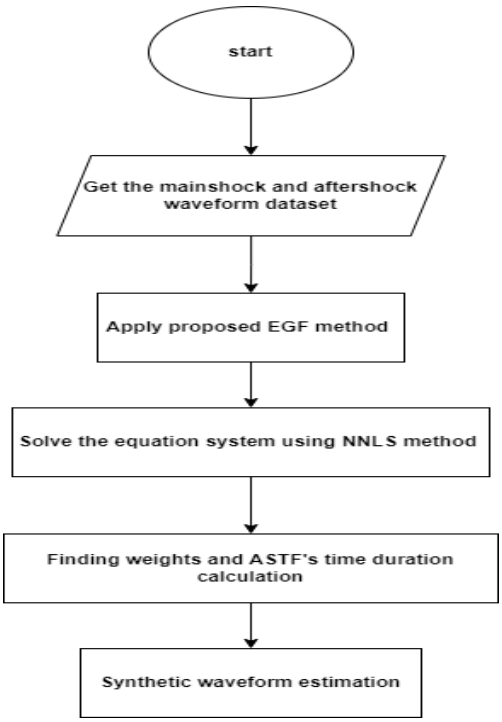

Figure 2. Schematic of the methodology.

4 Results

A FORTRAN code and GNU graphic scripts developed by (Plicka et al 2022). was used to get the results. The results here are for 4 stations around the epicenter of earthquake.

The results for each station are divided in to two figures. The three-component normalized waveforms and amplitude

spectra of the mainshock and EGF event are displayed by first set of Gnuplot script (Figs.3, 6). The numbers at the waveforms panel are the true amplitudes. The waveforms are filtered in the same frequency range as that used in the inversion. The frequency range is marked by the green zone in the amplitude-spectra plot.

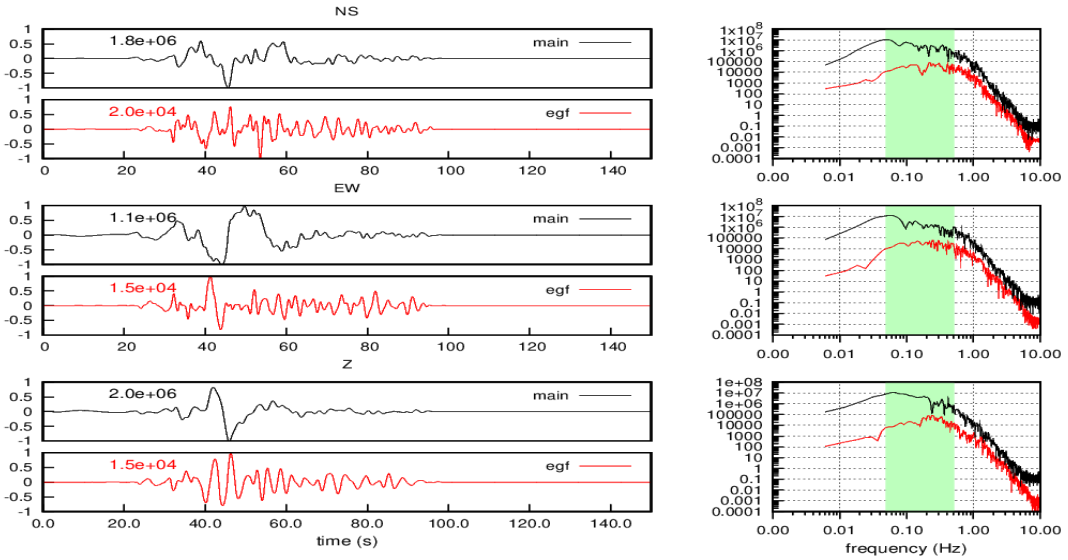

Figure 3. Normalized waveforms of mainshock (black) and EGF (red) waveforms (left) filtered in the frequency range from 0.05 to 0.5Hz (green zone). The numbers at waveform's panels are the maximum amplitudes (in counts). The left panels shows the acceleration time series for the mainshock and EGF event at each seismic station. Right panels are the corresponding Fourier amplitude spectra. The result of MRD station.

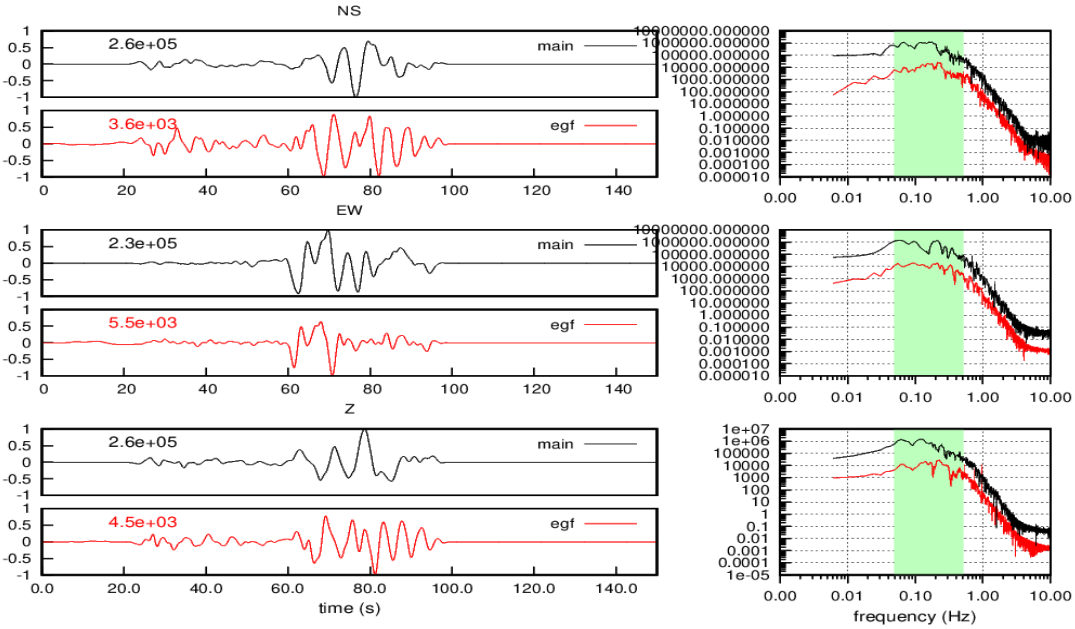

Figure 4. Same as figure 3 for SDS1 Station, filtered in the frequency range from 0.05 to 0.5Hz (green zone).

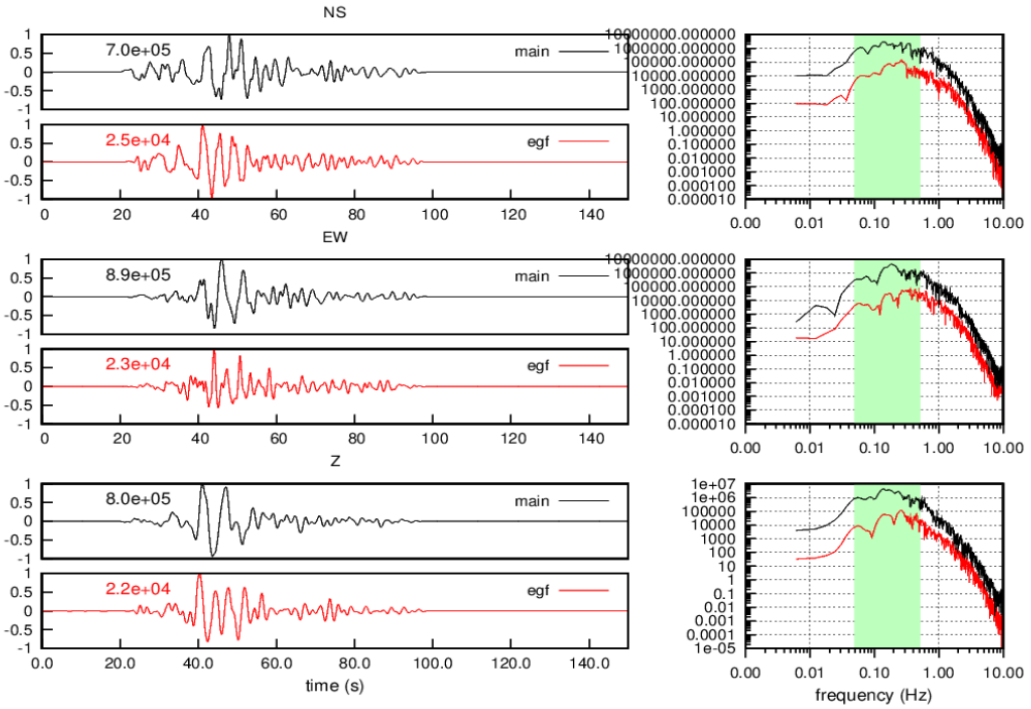

Figure 5. Same as figure 3 for URUN Station, filtered in the frequency range from 0.05 to 0.5 Hz (green zone).

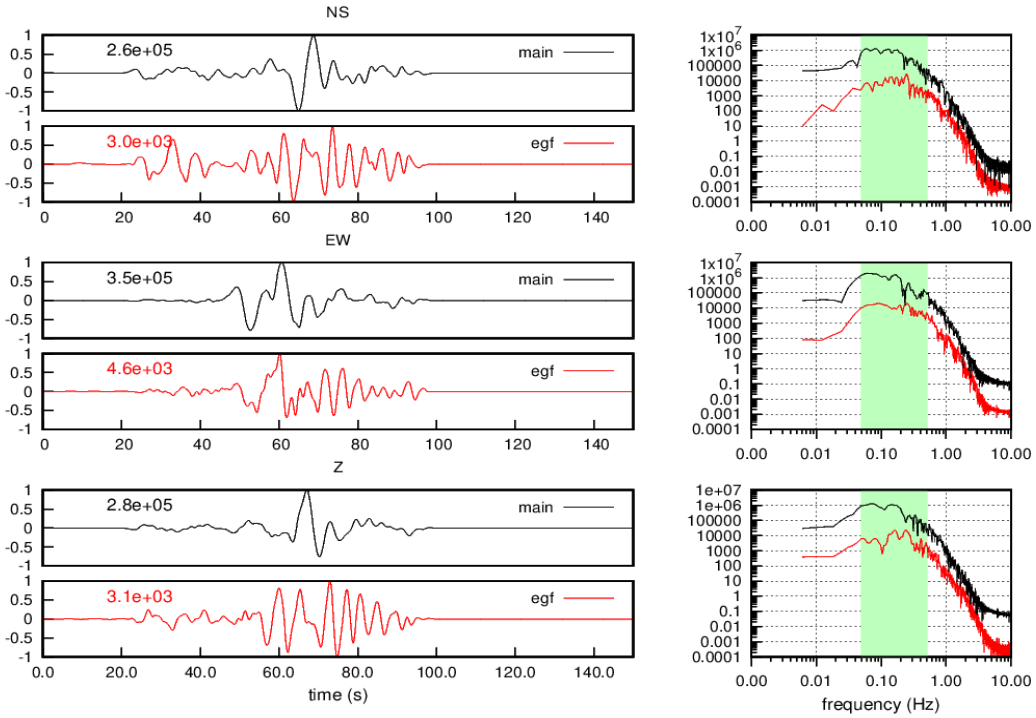

Figure 6. Same as figure 3 for MAHB Station, filtered in the frequency range from 0.05 to 0.5Hz (green zone).

The second series of outputs (Figs. 7, 10) includes a header that summarizes the general parameters, such as the station name, original or integrated input records, frequency band (in Hz), and seismic moment ratio. Additionally, this header displays the legend for the waveform panel.

The main result of the inversion, i.e., the weights, is shown in the top left panel within the time interval T=<t_1, t_2>. The figure below illustrates the moment rate function, constructed according to Eq. (3) using triangles with a width of $1/F_{max}$, as indicated in the legend along with the maximum moment rate value. The subsequent plot displays the cumulative sum of weights, which represents the moment function.

Synthetic seismograms at the right panel are calculated according to Eq. (4) for all estimated weights (red) and their subset $w_{J...K}$ (green) mentioned above. The numbers represent the true amplitudes and variance reductions for each component. Users can compare how the subset of weights fits the observed mainshock (blue) relative to the fit using all weights. This process helps identify redundant weights and removes the corresponding 'tail' of the ASTF as a noisy artifact. The amplitude spectra of the NS components for the EGF event (black), observed mainshock (blue), and synthetic mainshock (red) are located in the bottom left part of the figure.

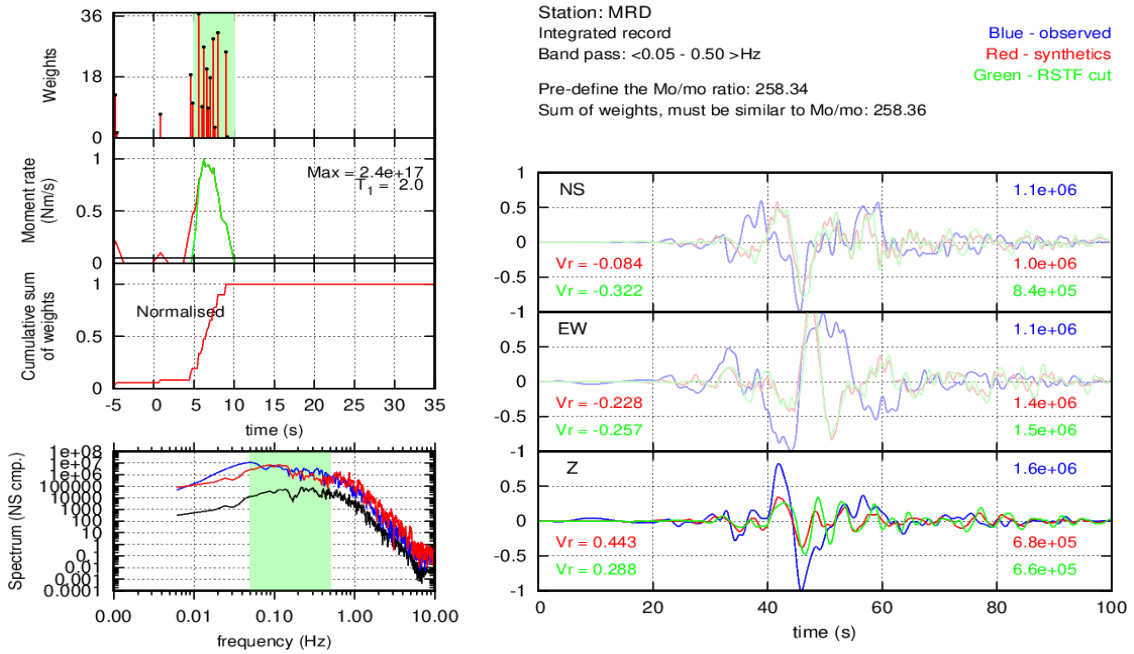

Figure 7. Summary plot of EGF method for MRD station where the frequency range used in the inversion is highlighted by the green zone in the amplitude spectrum. The Vr (Variance Reduction) for each component is displayed, quantifying the fit between the observed and synthetic waveforms. The RSTF cut indicates the portion of the Apparent Source Time Function (ASTF) that has been excluded due to noise or inaccuracies in the inversion process.

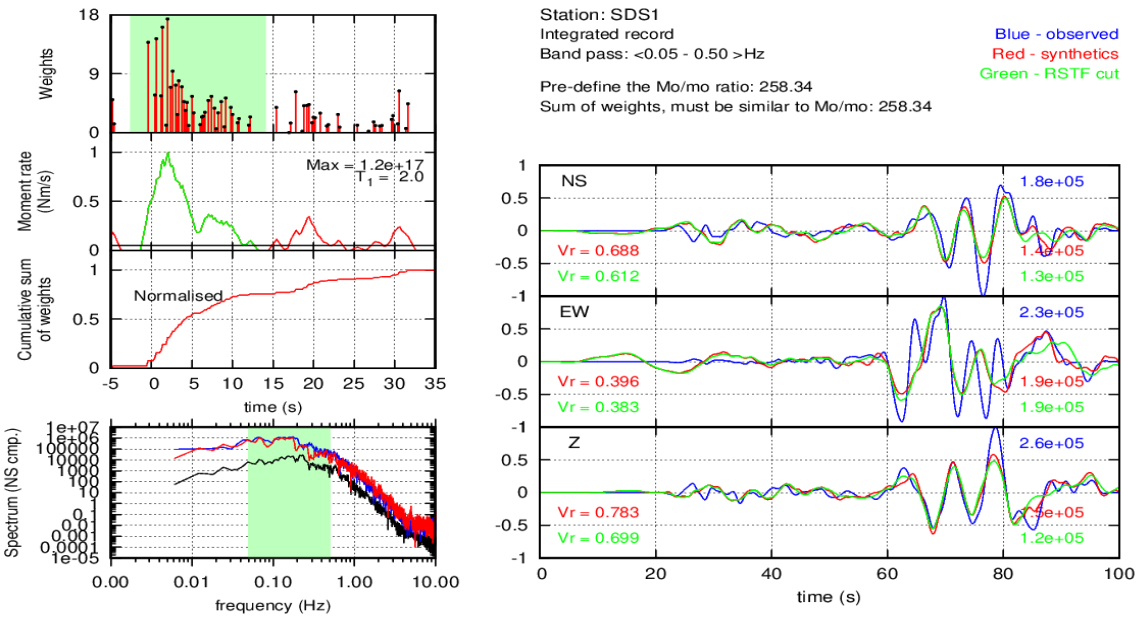

Figure 8. Summary plot of EGF method for SDS1 station.

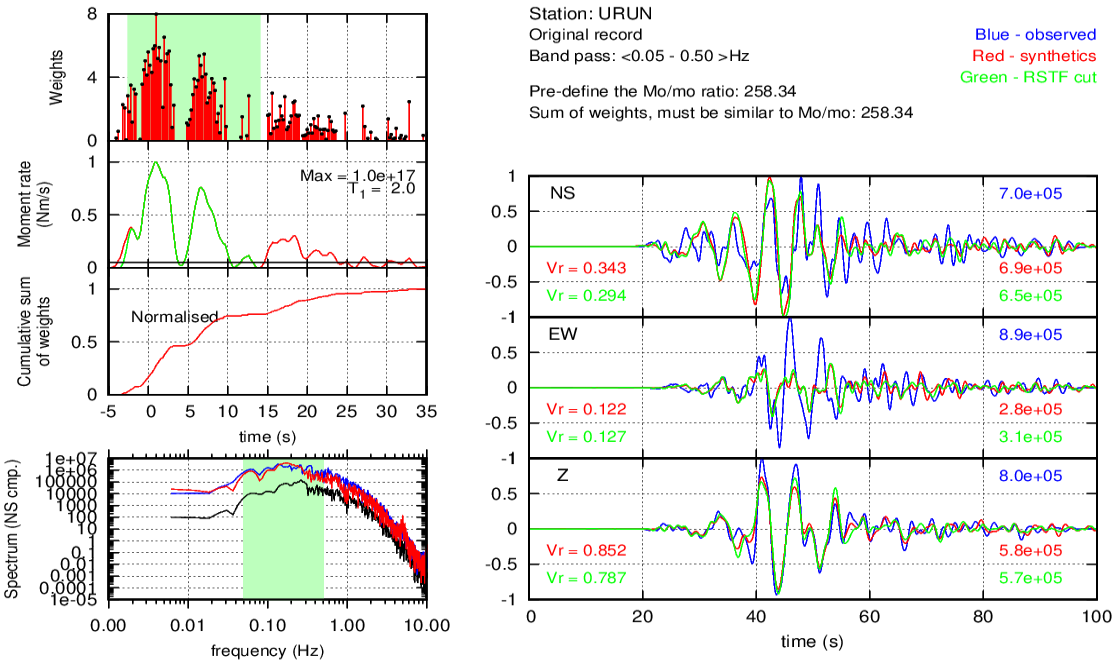

Figure 9. Summary plot of EGF method for URUN station.

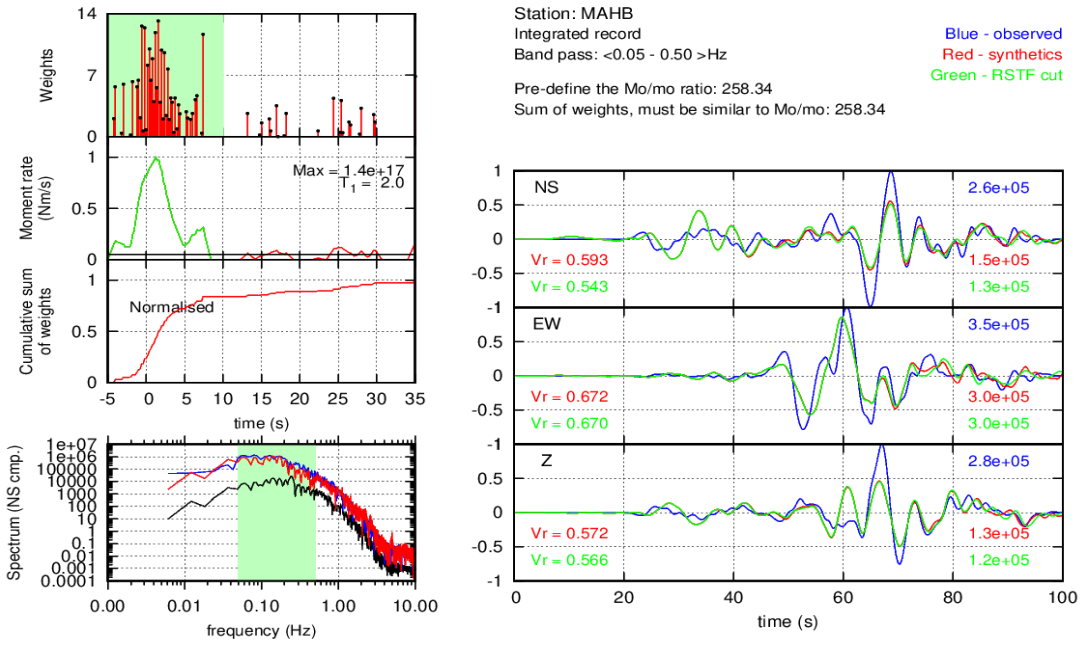

Figure 10. Summary plot of EGF method for MAHB station.

As it is obvious, from all of the stations mentioned here ASTF can be seen on the top left of the last four figures. For MRD station we find 5 seconds of ASTF, for SDS1 it is 15s, URUN for 18s and MAHB for 12s.

Using maximum amplitude for each component of each station, we also compare the fit between synthetic and green (ASTF) waveform to mention the quality of the method or estimation error for the mentioned method (table 3).

Table 3. Maximum amplitude in each station for each parameter which show to quality of the fit between the synthetic and Green waveforms.

Station	NS		EW		Z	
MRD	N/A		N/A		6.8e+05	6.8e+05
MAHB	1.5e+05	1.3e+05	3.0e+05	3.0e+05	1.3e+05	1.2e+05
SDS 1	1.4e+05	1.3e+05	1.9e+05	1.9e+05	1.5e+05	1.2e+05
URUN	6.9e+05	6.5e+05	2.8e+05	3.1e+05	5.8e+05	5.7e+05

Table 3 provides key indicators that reflect the quality of the Apparent Source Time Function (ASTF) results and the associated estimation error. These indicators are derived from the inversion process and offer insights into how well the synthetic waveforms match the observed data. The primary indicators of inversion quality include the weights, variance reduction, and the cumulative sum of weights, all of which are crucial for assessing the accuracy of the ASTF calculation.

The estimated weights represent the contributions of time-shifted Empirical Green's Function (EGF) records to the overall moment rate function. A good fit between the estimated moment rate function (constructed using these weights) and the observed waveforms

suggests low estimation error.

Variance reduction quantifies how well the synthetic waveform fits the observed data. Higher variance reduction indicates a better match and, consequently, a higher-quality result. A lower variance reduction would suggest that the synthetic waveform deviates significantly from the observed data, indicating higher estimation error.

The cumulative sum of weights provides insight into the consistency and smoothness of the inversion process. A smooth cumulative sum indicates well-constrained weights and a reliable ASTF estimate, while sharp irregularities may suggest a higher estimation error.

5 Conclusion and Discussion

As mentioned, the apparent source time function (ASTF) for this study was calculated to determine the characteristics of the seismic source that generated the earthquake. The ASTF represents the seismic signal recorded at a particular station and provides information about the duration, amplitude, and frequency content of the earthquake source, making its calculation crucial in seismology. In this study, the temporal distribution of seismic energy was calculated as ASTFs. The variation in ASTF duration among different stations is noteworthy. For instance, the MRD station shows a relatively short ASTF of 5 seconds, SDS1 has a longer ASTF of 15 seconds, and URUN is the longest ASTF with 18 second and MAHB with 12 seconds, respectively. These differences may reflect variations in fault properties, rupture dynamics, or local geological conditions near each station.

The variation in Apparent Source Time Function (ASTF) durations observed across the four seismic stations in this study can potentially be linked to their relative positions with respect to the North Tabriz Fault, the causative fault of the Khoy earthquake. As shown in Figure 1, the stations are distributed at varying distances from the fault trace, which could significantly influence the characteristics of the recorded seismic signals. Stations that are closer to the fault, such as MRD and URUN, are likely to record faster seismic arrivals with shorter ASTF durations. In contrast, stations farther from the fault, such as SDS1 and MAHB, may capture more complex seismic waveforms, resulting in longer ASTF durations due to the increased distance over which seismic waves travel. This difference could be attributed to the time it takes for seismic energy to propagate from the rupture source to each station.

Additionally, the rupture propagation direction along the right-lateral strike-slip North Tabriz Fault is another important factor to consider (Salmanian, et al. 2025). The direction of rupture propagation relative to station locations may influence the duration and complexity of the observed seismic signals. For instance, the URUN station, located southeast of the fault, is closer to the direction of rupture propagation, which could result in a longer ASTF duration, as the rupture may have propagated more directly towards this station. Stations farther from the rupture zone or located in different azimuthal directions, such as SDS1 and MAHB, might observe less direct rupture propagation, leading to shorter ASTFs. This observation is in line with the findings of Plicka et al. (2022), where ASTF durations were influenced by the station positions relative to the rupture zone. Overall, the differences in ASTF durations across the stations in this study

likely reflect a combination of their proximity to the fault, the direction of rupture propagation, and the local geological conditions, all of which contribute to the observed seismic waveforms.

The findings have direct implications for seismic hazard assessment in the Khoy region. Longer ASTFs (e.g., SDS1) indicate more extended rupture durations, potentially leading to stronger ground shaking. Shorter ASTFs (e.g., MRD) may correspond to less energetic ruptures. The rupture propagates toward the MRD station (azimuth ~60-80 degrees), evidenced by the very short duration and large amplitudes of the ASTF. The other stations (azimuth ~150-170 degrees) are not in the rupture's direction, resulting in less significant earthquake damage in these areas. Geological features influence ASTFs; for example, stations near fault segments with high stress accumulation may exhibit longer ASTFs due to larger fault areas involved in the rupture. Stations on softer sediments might experience more prolonged shaking due to energy-trapping effects. Future studies can emphasize investigating correlations between ASTFs and fault properties (e.g., frictional strength, fault geometry) and exploring how local geological heterogeneities affect ASTFs.

In conclusion, this work advances the knowledge of earthquake source parameters through detailed ASTF analysis. By highlighting the station-specific variations and their implications, we underscore the importance of this research for seismic hazard assessment and fault characterization in the Khoy region.

References

Courboulex, F., J. Virieux, A. Deschamps, D. Gibert and A. J. G. J. I. Zollo (1996). "Source investigation of a small event using empirical Green's functions and simulated annealing." **125**(3): 768-780.

Hough, S., J. Lees and F. J. B. o. t. S. S. o. A. Monastero (1999). "Attenuation and source properties at the Coso Geothermal Area, California." **89**(6): 1606-1619.

Hough, S. J. J. o. G. R. S. E. (1997). "Empirical Green's function analysis: Taking the next step." **102**(B3): 5369-5384.

Hutchings, L., G. J. E. R. Viegas and A.-N. F. i. Seismology (2012). "Application of empirical Green's functions in earthquake source, wave propagation and strong ground motion studies." 87-140.

Hutchings, L. J. B. o. t. S. S. o. A. (1991). "“Prediction” of strong ground motion for the 1989 Loma Prieta earthquake using empirical Green's functions." **81**(5): 1813-1837.

Irikura, K. (1984). Prediction of strong ground motions using observed seismograms from small events. Proc. 8th World Conf. on Earthq. Eng.

López-Comino, J. Á., F. d. L. Mancilla, J. Morales and D. J. G. R. L. Stich (2012). "Rupture directivity of the 2011, Mw 5.2 Lorca earthquake (Spain)." **39**(3).

Mueller, C. S. J. G. R. L. (1985). "Source pulse enhancement by deconvolution of an empirical Green's function." **12**(1): 33-36.

Plicka, V., F. Gallovič, J. Zahradník, A. Serpetsidaki, E. Sokos, N. Vavlas and A. J. T. Kiratzi (2022). "The 2020 Samos Mw7 earthquake: Source model depicting complexity and rupture directivity." **843**: 229591.

Salmanian, M., A. Rastbood and M. M. J. J. o. A. E. S. Hossainali (2025).

"Evaluating interseismic deformation patterns in the North Tabriz Fault (Iran) using enhanced fitting of velocity field and analysis of surface deformation." **277**: 106376.

Salmanian, M., A. Rastbood and M. M. J. J. o. G. S. Hossainali (2024). "Estimating the slip rate in the North Tabriz Fault using focal mechanism data and GPS velocity field." **14**(1): 20220167.

Stein, S. and M. Wysession (2009). An introduction to seismology, earthquakes, and earth structure, John Wiley & Sons.